the slots of the rotor. The flux-weakening is obtained supplying de field winding in a manner as to create an opposite flux to the permanent magnet flux. Similarly, by changing the current direction in the additional winding a flux-strengthening can be obtained. The stator and rotor armatures have to be manufactured of very good quality laminations in order to minimize the effects of saturation. The flux weakening also means reducing the iron losses.

In order to avoid the slip rings in the rotor in the case of the second variant in study the field winding was moved on the interior stator of the HSM (see Fig. 2). In this case the flux changing is performed exactly in the same manner as it was presented previously.

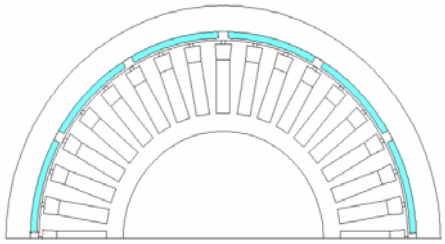

a) cross-section

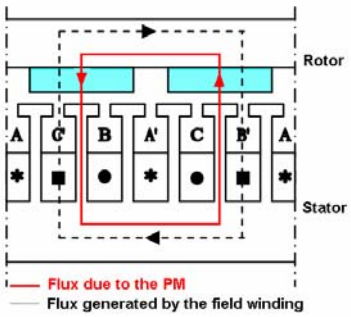

b) flux pattern

Fig. 2. HSM variant with SPM rotor and additional field winding on stator.

The third HSM structure considered is similar to the second one, with the single difference that the rotor has interior permanent magnets (IPM) in a flux concentrated pattern. Because the performances of this variant depends strongly on the rotor number of poles, several cases were taken into study in the range of 4÷16 poles.

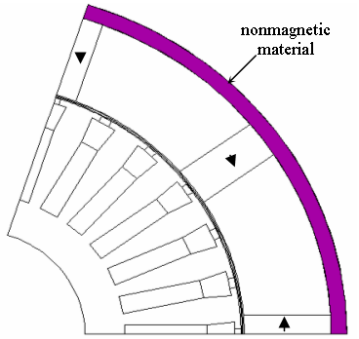

Fig. 3. HSM variant with IPM rotor and additional field winding on stator.

From the numerous results obtained, under a 2D finite element method (FEM) analysis done on the HSM variants, with the same main dimensions, only three shaded colour plots of the magnetic flux densities in the considered variants, which are quite representative, are given in Fig. 4.

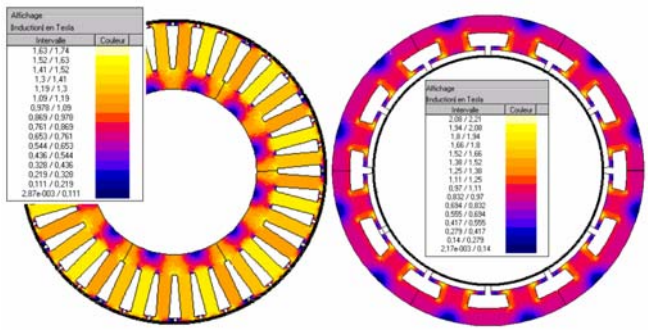

a) first variant

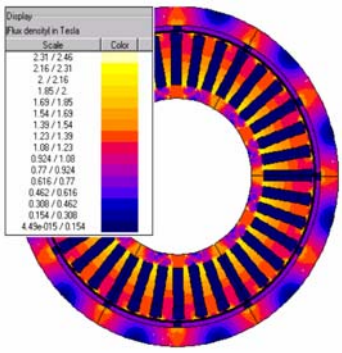

b) second variant

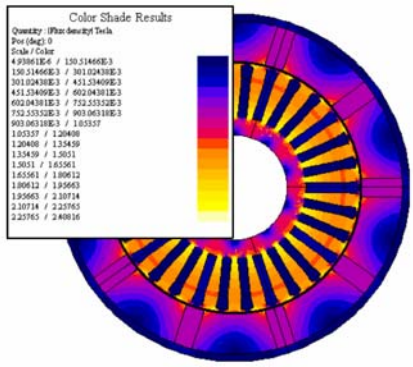

c) third variant

Fig. 4. The shaded colour plots of the magnetic flux densities.

To compare the three HSM variants their main characteristics were computed analytically and by means of FEM analysis.

The efficiency, the power density, the active parts weight / costs ratio, the permanent magnet's weight, the flux weakening capabilities and the existence of the sliding contact were the main analysed characteristics. In the case of the variant with IPM rotor and flux concentrating topology, the best structure, that having 8 pole pairs, was taken into account.

The main results of this comparative study are given in Table I.

TABLE I
MAIN PARAMETERS OF THE HSM VARIANTS

Item	HMS variant		
	1	2	3
Efficiency	88%	83%	78%
Output power / weight	5.5 kW / 28.2 kg	5.5 kW / 36.8 kg	5.5 kW / 95 kg
Weight / costs of active parts	28.2 kg / 423 €	36.8 kg / 641 €	95 kg / 1400 €
Magnet's weight	1.8 kg	3.6 kg	15.3 kg
Flux weakening capability	Good	Medium	Weak
Sliding contact	Yes	No	No

As it can be seen from the Table 1, the first variant has the best performances regarding almost all the characteristics The single drawback of this HSM variant is the existence of the slip rings-brushes system.

Taking into account the above study on the performances of the three HSM variants, respectively the possibilities to construct the machine, the first variant was chosen and an inner rotor construction prototype resulted. The constructed prototype is presented further.

III. HSM IN A GENERATING REGIME

ISG is operating mainly as a generator to supply the consumers and to charge the battery. Therefore here some theoretical developments concerning the hybrid synchronous generator (HSG) are presented.

The HSG mathematical model, considering, for the sake of generality, the rotor excitation fields on both *d*- and *q*-axis, is [9]:

$$\begin{aligned} v_d + Ri_d &= \omega\lambda_q \\ v_q + Ri_q &= -\omega\lambda_d \\ \lambda_d &= L_d i_d + \lambda_{fd} \\ \lambda_q &= L_q i_q + \lambda_{fq} \end{aligned} \tag{1}$$

or, with general state vectors,

$$\begin{aligned} \underline{v_s} + R\underline{i_s} &= -j\omega\underline{\lambda_s} \\ \underline{\lambda_s} &= \lambda_d + j\lambda_q = L_d i_d + jL_q i_q + \lambda_{fd} + j\lambda_{fq} \end{aligned} \tag{2}$$

The motoring regime mathematical model can be obtained from the generator's one by simply considering the change of the power circulation from the source to the machine, when for generator it is on the opposite direction [10].

The vectors' diagram in generator regime is given in Fig. 5.

The notations are the usual ones,

- v_d, v_q; i_d, i_q; λ_d, λ_q; L_d; L_q; are *d* and *q*-axis voltages, currents, flux linkages and synchronous inductances respectively.
- ω is rotor speed, equal with the stator **emf** pulsation for one pole pair machine.

The induced **emf**s are [11]:

$$\begin{aligned} E_{0d} &= -j\omega\lambda_{fd} \\ E_{0q} &= -j\omega(j\lambda_{fq}) \end{aligned} \tag{3}$$

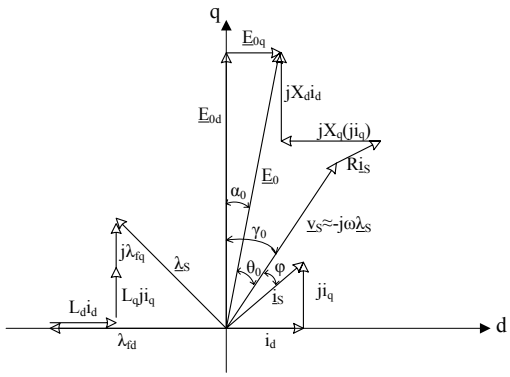

Fig. 5. Vectors' diagram, HSG steady-state regime.

Neglecting the stator phase resistance the scalar equations are:

$$\begin{aligned} E_{0d} &= V_s \cos\gamma_0 + X_d I_d \\ E_{0q} &= V_s \sin\gamma_0 - X_q I_q \\ X_d &= \omega L_d \\ X_q &= \omega L_q \\ \gamma_0 &= \alpha_0 + \theta_0 \\ I_d &= I_s \sin(\gamma_0 + \varphi) \\ I_q &= I_s \cos(\gamma_0 + \varphi) \end{aligned} \tag{4}$$

A general case of a HSG operating on a symmetrical load with an electronically controlled (EC) LC block on each phase for voltage control is considered, Fig. 6.

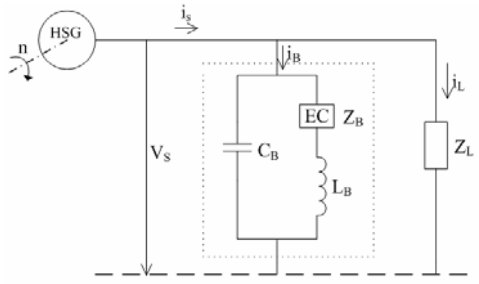

Fig. 6. HSG load and EC block on one phase.

The phase currents, and impedance, are:

$$\begin{aligned} \underline{I_s} &= \underline{I_B} + \underline{I_L} \\ \underline{I_s} &= \underline{V_s}\left(\frac{1}{\underline{Z_B}} + \frac{1}{\underline{Z_L}}\right) \\ I_s &= V_s \frac{Z}{Z_L Z_B} \\ Z &= \sqrt{\left(\frac{R_B Z_L}{Z_B} + \frac{R_L Z_B}{Z_L}\right)^2 + \left(\frac{X_L Z_B}{Z_L} + \frac{X_B Z_L}{Z_B}\right)^2} \end{aligned} \tag{5}$$

where R_L, R_B, X_L, X_B, Z_L, Z_B are load, respectively LC block resistances, reactances and impedances.

After some simple mathematical calculations results:

$$\cos\varphi = \frac{V_s(1-X_q/X_d)\sin\gamma_0\cos\gamma}{V_s\dfrac{Z}{Z_L\cdot Z_B}X_q} + \frac{E_{0d}X_q/X_d\sin\gamma_0 - E_{0q}\cos\gamma_0}{V_s\dfrac{Z}{Z_L\cdot Z_B}X_q} \quad (6)$$

The power factor can be equal to unity due to the electronic converter placed between HSG and the load,

$$V_s = \frac{E_{0d}\,X_q/X_d\sin\gamma_0 - E_{0q}\cos\gamma_0}{\dfrac{Z}{Z_LZ_B}X_q - (1-X_q/X_d)\sin\gamma_0\cos\gamma_0} \quad (7)$$

If the HSG has a reduced saliency, then:

$$X_d \cong X_q = X_s$$

$$V_s = \frac{E_{0d}\sin\gamma_0 - E_{0q}\cos\gamma_0}{\dfrac{Z}{Z_LZ_B}X_s} \quad (8)$$

It is clear that the *d*-axis excitation field acts in the same manner as the *q*-axis excitation field, therefore there is no reason to have both excitation windings. Without the *q*-axis excitation field the product between output HSG phase voltage and power factor comes as:

$$V_s\cos\varphi = \frac{E_{0d}\sin\gamma_0}{\dfrac{Z}{Z_LZ_B}X_s} \quad (9)$$

In an ISG case there is no need for an electronically controlled LC block since the voltage can be controlled only via *d*-axis variable field and via the electronic converter existing between the HSG and the load.

A general equation where the phase terminal voltage is given in function of load current I_S, power factor, induced phase **emf** and HSG parameters comes after some mathematical developments as:

$$\sqrt{\left(V_S + I_SX_q\sin\varphi\right)^2 + \left(I_SX_q\cos\varphi\right)^2}\,E_0 = V_S{}^2 + V_SI_S(X_d + X_q)\sin\varphi + X_dX_qI_S{}^2 \quad (10)$$

Of course (10) would be simplified in the case of the ISG since the power factor is maintained almost equal to unity.

IV. HSM PROTOTYPE AND TESTS

A specific design procedure was developed based on existing literature, as [12, 13, 14]. Using that specific procedure and employing a lot of 2D FEM calculations, a HSM prototype was designed, constructed and tested [14]. The simplest solution was chosen, the permanent magnets (PMs) and the auxiliary winding on the interior rotor.

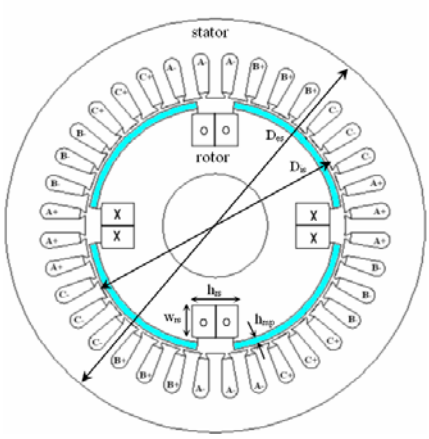

Fig. 7. HSM prototype cross section.

The cross section of the HSM prototype is shown in Fig. 7, and a detailed view of its rotor in Fig. 8.

Fig. 8. HSM prototype rotor.

The adopted solution has the advantage that many parts from a wound rotor induction motor could be used. The stator core was made a bit longer than that of the induction motor, the stator winding was changed accordingly to the calculation done for HSM and the rotor was entirely new constructed, but using the mechanical parts and the iron core steel sheets of the original induction motor. The main dimensions of the machine are given in Table II.

TABLE II
HSM MAIN DIMENSIONS

Symbol	Quantity	Value
L	Motor's length	100 mm
D_{es}	Outer stator diameter	200 mm
D_{is}	Inner stator diameter	124 mm
g	Air-gap length	1 mm
h_m	Permanent magnet's thickness	3.5 mm
θ_{pm}	Permanent magnet angular width	72°
h_{ss}	Stator slot height	21.8 mm
h_{rs}	Rotor slot height	17 mm
w_{rs}	Rotor slot width	22 mm

The HSM parameters, obtained by tests or by 2D-FEM calculation are:

– Stator phase resistance $R = 1.7745\ \Omega$,
– Stator phase leakage inductance $L_\sigma = 0.004975$ H,
– d-axis synchronous inductance $L_d = 0.02028$ H,
– q-axis synchronous inductance $L_q = 0.01586$ H.

The rated output power, when operating as a generator, is 5.16 kW at rated phase voltage $V_s = 200$ V and rated phase current $I_s = 8.6$ A for unity power factor. Due to the imposed stator slot area the number of turns and the rated current had to be kept almost as for the original induction motor and consequently the prototype output voltage is much larger than the one required for an ISG. Anyway the prototype proved fully useful since it allowed for checking the design procedure and of all machine computed characteristics.

A lot of tests were performed on the prototype, some, concerning the generating regime being given here.

A comparison between phase **emf** values, 2D-FEM calculated, respectively test obtained, at no load is given in Fig. 9.

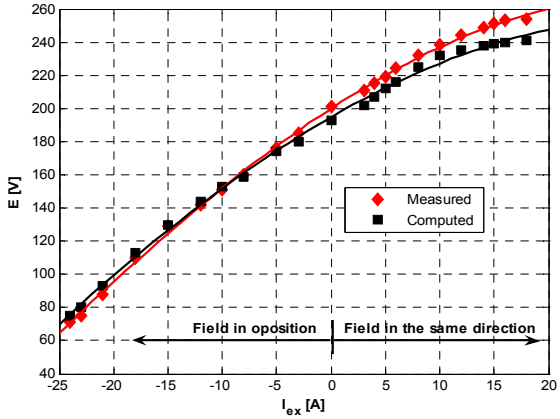

Fig. 9. 2D-FEM and tests values, induced stator phase emf.

From the numerous terminal characteristics plotted based upon the computed, respectively measured results, here only two sets will be presented: those obtained at unitary power factor and $I_{ex} = 0$ A, respectively $I_{ex} = 2.5$ A, Fig. 10.

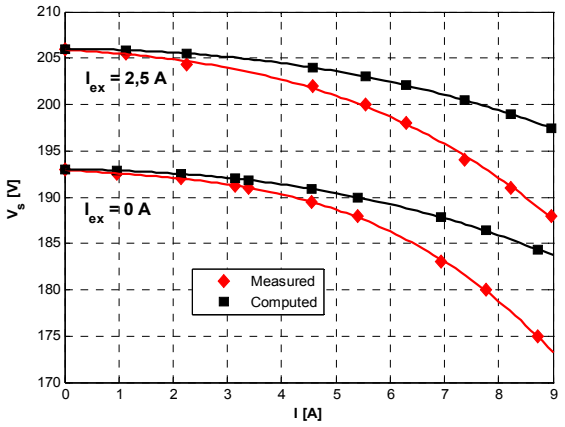

Fig. 10. Output voltage plotted upon measured and computed data.

A very interesting characteristic, concerning the behaviour of the HSG in a large load domain is given in Fig. 11.

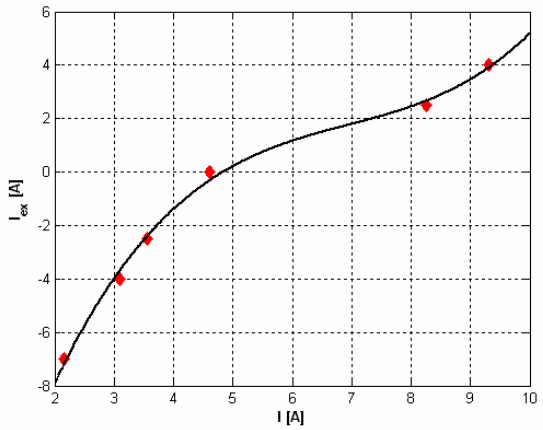

Fig. 11. HSG prototype excitation current vs. load current, phase voltage 190 V, unity power factor.

From the characteristic given in Fig. 11 one can see that at a very large variation of the load the output voltage can be maintained constant by varying the auxiliary field winding current. That is an important advantage of a HSM and it should be very carefully considered.

A similar characteristic can be obtained for a large speed domain, when the output voltage is maintained almost constant against the speed and load variation.

V. Field Weakening, HSM Motoring Regime

In the case of permanent magnet synchronous motors there is only one possibility to weaken the field, and, consequently to increase the speed domain, creating a d-axis stator flux opposite to the rotor field flux. In the case of SPM rotor synchronous motor the speed domain can be doubled, at maximum, through this method. It is quite un-sufficient for an ISG, besides the fact that it means additional losses produced in the stator winding and an important increase in the electronic converter current.

A comparison between the two ways of producing the flux weakening, via d-axis stator current and respectively additional field winding, can be made in the case of HSM.

Suppose that the length and the cross section of the stator and rotor winding are the same then $R/R_f = N/N_f$. In consequence the joule losses in flux-operating, with d-axis current injection and auxiliary excitation current, when the resulting air-gap flux is the same, are:

$$\frac{p_{jd}}{p_{jf}} = \frac{R}{R_f}\cdot\frac{i_d^2}{I_f^2} \cong \left(\frac{N_f}{N}\right)^3 \Rightarrow p_{jd} = p_{jf}\cdot\left(\frac{N_f}{N}\right)^3 \qquad (11)$$

It results, within these simplifying assumptions, which are not far of the reality, that the stator supplementary losses are much larger when the d-axis current is employed, for the flux weakening, than the auxiliary field winding losses at the same flux.

Thus, the efficiency is improved at the same speed gain,

since obviously the field winding number of turns is, or should be, larger than the stator phase number of turns. It can be seen from the simulations shown in Fig. 12, when the same speed increase was obtained.

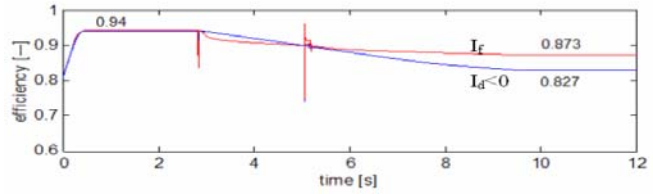

Fig. 12. Efficiency when HSM operates in a flux weakening regime ($I_d < 0$ or I_f).

In the following a flux weakening dynamic regime simulation, for the case when only the additional field current is employed, is presented.

The simulations were performed for a 5500 W, 1500 rpm, 48 Vcc sample HSM, with 12 poles, and a rated current of 81.3 A.

Its phase parameters are: the resistance 0.017 Ω; the *d-q* axis inductances $2.858 \cdot 10^{-5}$ H, $2.142 \cdot 10^{-5}$ H, respectively.

During the simulated dynamic regime the HSM was started, up to its rated speed, and after some time its speed was increased using flux weakening. The results of the simulation are given in Fig. 13 and they clearly evinced the speed increase due to the auxiliary field winding current presence.

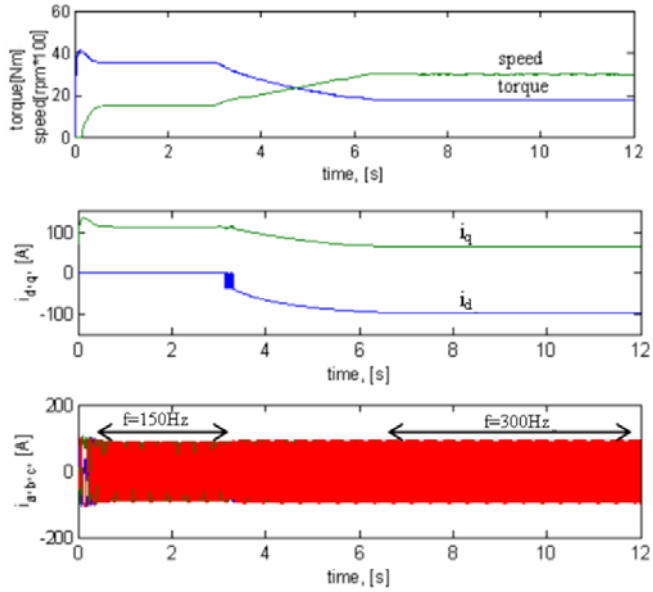

Fig. 13. The torque, speed and current in flux weakening with auxiliary field current I_f different to zero.

As a matter of fact on the constructed prototype, within all the implicit limitations due to the use of an induction motor structure, the speed domain was extended more than three times, considering the base speed the one that corresponds to synchronous speed at 50 Hz.

VI. Conclusions

A HSM was presented as an alternative solution for ISG in hybrid and mild hybrid automobiles. Three HSM variants were analyzed. The best variant resulted that having both field sources, PMs and the additional field winding, on the rotor.

For this variant a prototype was designed, constructed and tested. The paper presents also some analytical developments and simulation results, beside the tests and the data concerning the prototype.

From all the developments and results presented a main conclusion is at hand: the HSM can be a very good choice for an ISG in hybrid cars since it has good power density, significant starting torque and large enough speed domain.

Moreover due to the possible field control in a generating operating mode, the output voltage can be largely controlled and therefore the electronic converter does not have to be designed for quite high voltages which could be generated at high speeds.

References

[1] I. Husain, "*Electric and hybrid vehicles. Design fundamentals*," CRC Press LLC, Boca Raton (Fl, USA), 2003.

[2] T. Lipman, R. Hwang, "Hybrid electric and fuel cell vehicle technological innovation: hybrid and zero-emission vehicle technology links," *Proc. of the 20th International Electric Vehicle Symposium and Exposition*, Long Beach (CA, USA), 2003, pp. 111-119.

[3] M. Comanescu, A. Keyhani, M. Dai, "Design and analysis of 42-V permanent-magnet generator for automotive applications," *IEEE Trans EC*, vol. 18 (2003), no. 1, pp. 107-112.

[4] A.G. Jack, B.C. Mecrow, C. Weiner, "Switched reluctance and permanent magnet motors suitable for vehicle drives – a comparison, *Proc. of the International Electric Machines and Drives Conference (IEEE IEMDC '99),* Seattle (USA), 1999, pp. 345-350.

[5] I.-A Viorel, G. Henneberger, R Blissenbach, L. Löwenstein, "*Transverse flux machines. Their behaviour, design, control and applications,*" Mediamira, Cluj (Romania), 2003.

[7] X. Luo, T.A. Lipo, "A synchronous permanent magnet hybrid ac machine," *Proc. of the International Electric Machines and Drives Conference (IEEE IEMDC '99),* Seattle (USA), 1999, pp. 19-21.

[6] C. Mi, "Rare-Earth Permanent Magnet Machines for Automotive Applications," *Proc. of the 2nd Annual Winter Workshops Series*, Vetronics Institute, College of Engineering and Computer Science, University of Michigan–Dearborn, Dearborn (MI, USA), 2002, pp. 234-241.

[8] D. Fodorean, I.A. Viorel, A. Miraoui, M. Gutman, "Comparison of hybrid excited synchronous motors for electrical vehicle propulsion," *Proc. of Aegean Conferences on Electrical Machines and Power Electronics ACEMP '04*, Istanbul (Turkey), 2004, pp. 52-57.

[9] S. Scridon, I. Boldea, L. Tutelea, F. Blaabjerg, A.E. Ritchie "BEGA – a biaxial excitation generator for automobiles: comprehensive characterization and test results," *IEEE Trans. IA*, vol. 41 (2005), no. 4, pp. 935-944.

[10] D. Fodorean, A. Djerdir, A. Miraoui, I.-A. Viorel, "Flux weakening performances for a double-excited machine" *Proc. of ICEM '04*, Krakow, Poland, 2004, paper no. 434 on CD-ROM.

[11] G. Henneberger and I.-A. Viorel, "*Variable reluctance electrical machines*," Aachen (Germany), Shaker Verlag, 2001.

[12] J.F. Gieras and M. Wing, "*Permanent magnet motor technology, design and applications*," New York Marcel Dekker, 1997.

[13] D.C. Hanselmann, "*Brushless permanent magnet motor design*," New York McGraw-Hill, 1994.

[14] G. Henneberger, J.R. Hadji-Minaglou, R.C. Ciorba, "Design and test of permanent magnet synchronous motor with auxiliary excitation winding for electric vehicle application" *Proc. of EPE Chapter Symposium*, pp. 645-649, Lausanne, 1994.